RESEARCH ARTICLE

Effect of Sintering condition on Magnetization and Microstructure of $Cu_xCo_{(1-x)}Fe_2O_4$ Ferrites

K.P. Mudholakar[1], S.Vinaykumar[1], VinutV.Tambe[1], S.V. Angadi[1], S.S. Kakati[2], Shridhar N.Mathad[2*], Sachin S.Tirlapur[1], I.B Madalagi[1], Deepak B. Shirgaonkar[3], A.S. Pujar[4], S.L.Galagali[4], P.R. Jeergal[1], S.S.Khemalapure[5],C.S.Hiremath[6], R.B.Pujar[1]

[1]Department of Physics, P.C.Jabin Science College, Hubballi, India
[2] Department of EngineeringPhysics, K.L.E Institute of Technology, Hubballi, 580027
[3]Department of Physics, Anandibai Raorane Arts, Commerce and Science College, Vaibhavwadi, Maharastra, 416810, India
[4]Department of Physics, R.L.S. Institute, Belagavi
[5]Department of Physics, K.L.E Society's Jagadguru Tontadarya (J.T.) College, Gadag, Karnataka.582101
[6]Department of Physics, S.K. Arts and H.S.Kotambari Science Institute, Hubballi, India

ABSTRACT: Nowadays, ceramic magnets are produced artificially under precisely managed sintering and compositional circumstances. As a result, copper doped cobalt ferrites with the general chemical formula $Cu_xCo_{(1-x)}Fe_2O_4$ (x=0.0, 0.4, and 1.0) were made using the standard ceramic method under varied sintering conditions using AR grade oxides. The formation of a single-phase spinel structure is demonstrated by X-ray diffraction. The morphological investigation, which indicates that densification, causes grains to develop and the magnetic characteristics, which suggest that lower sintering temperatures cause increase in magnetization, were carried out as part of the characterization processes.

KEYWORDS: ferrites, microstructure, magnetization, sintering condition.

https://doi.org/10.29294/IJASE.9.2.2022.2678-2685

1. INTRODUCTION

Ferrites are ceramic magnetic materials based on iron oxide that exhibit ferromagnetic behaviour. Ferrites' compositions and sintering conditions can be modified to alter their magnetic characteristics. Ferrites can be used in a variety of applications, and factors like permeability, coercivity, remanence, and saturation magnetization can help determine which applications. The spinel structure is physically flexible, which results in a wide range of physical properties and hence useful applications in many frequency ranges. The magnetic characteristics of ferrites are mostly influenced by the porosity and grain size [1-4]. Faraz et al [4] used two-sub lattice model to show ferrite magnetization. As a result, magnetic ions with uneven magnetic moments in the opposing directions inhabit the A and B sublattices. The resultant magnetization is caused by the different magnetic moments of sublattices A and B.

According to Weiss [5], there are magnetic domains, and each domain's magnetization is caused by the Weiss molecular field, which tends to arrange atomic dipoles in parallel. The specimen becomes spontaneously magnetized as a result of the vector sum of its domains [6]. By connecting magnetic ions by electron transfer via intermediate anions, Andersondeveloped the super exchange interaction to explain the magnetization in normal and inverse spinel ferrites [7]. Grain size, grain orientation, grain boundaries, pores, inclusions, and crystal flaws are the most crucial aspects of microstructure. Grain direction favours maximal BH, and grain boundaries act as current barriers and internal lamellae to limit eddy current losses. By generating depolarization zones that cause a drop in magnetization, the porosity pinning the domain

**Corresponding Author: physicssiddu@gmail.com*
Received: 15.08.2022 **Accepted:** 27.09.2022 **Published on**: 01.11.2022

wall motion and introducing internal inhomogeneous magnetic field [8,9].Several routes have been employed to prepare ferrites such as sol-gel auto combustion method [10-11], Co-precipitation method [12-13], aerosol method [14] and sucrose precursor sol-gel combustion [15], andsolid state method [16] and microwave method [17] and oxalate precursor method [18]. Compared to the wet powder preparation routes, the solid-state route is comparatively inexpensive and postulates simple apparatus and facilitates large volumes of powder can be prepared. The obtained powder demonstrates relatively high agglomeration, and large particle size as well as relatively limited homogeneity. The main objective of our work is to synthesize the $Cu_xCo_{(1-x)}Fe_2O_4$ (x=0.0, 0.4, and 1.0) by standard ceramic method. Systematic structural study has been performed by XRD, SEM and Magnetic Properties characterizations.

2. EXPERIMENTAL

In the present case, ferrites with general chemical formula $Cu_xCo_{1-x}Fe_2O_4$,where x= 0.0,0.4 and 1.0, were synthesized by standard ceramic method.Generally for solid state method all copper oxides, cobalt oxide and ferric oxides in stoichiometry, compositional weights of AR grade oxide powders were mixed physically in molar proportion and blended in agate mortar in acetone medium (with 99.90% purity)[19]. After drying, the mixture was sintered at 800^0 and 900^0 C for 20 and 30 hours in muffle furnace. The pre sintered powders were subjected to hard milling process in acetone medium. Structural, magnetic properties and Scanning Electron Microscope of synthesized materials were characterized after each sample then all sample applied for palletisation process with applying a pressure about 5 tons per square inch for 5 minutes by keeping the powder of about 1 gram in a die of 1 cm in diameters. The final sintering was carried out on pellets to complete the solid state reaction [19].The schematic presentation of work is shown in Fig.1

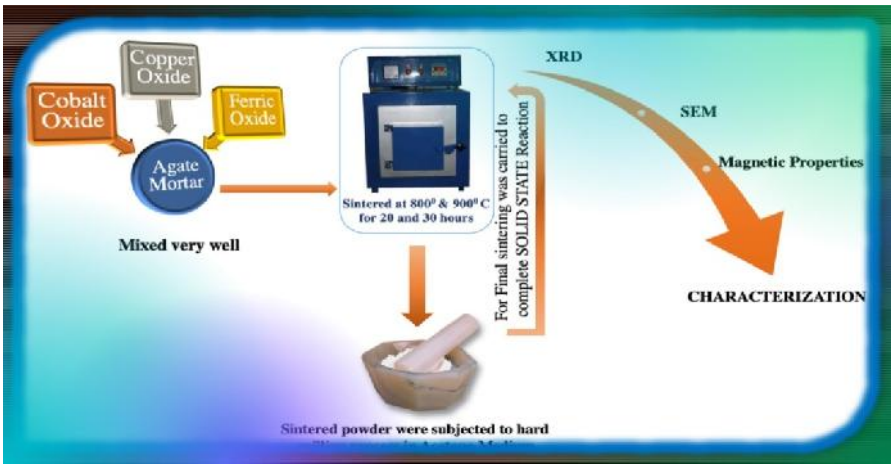

Figure 1 Synthesis method standard ceramic method

3. RESULTS AND DISCUSSION

3.1 X-ray diffraction and structural studies

The X-ray diffraction patterns of the samples were obtained from RSIC, University of Nagpur to confirm the formation of single-phase ferrites (Fig.2), by using Fe k-α radiation of wavelength 1.9360 A^0. The saturation magnetization of a standard nickel sample was used to calibrate the hysteresis loop and calibration factor was calculated by the relation. Cobalt ferrite, copper ferrite, and $Cu_{0.4}Co_{0.6}Fe_2O_4$ made using the solid-state technique were the materials tests. By using stoichiometric amounts of cobalt oxide, cuprous oxide, and ferric oxide and then grinding them for 4 hours in an agate mortar in acetone medium, the necessary composition can be achieved. Following drying, the mixture was sintered in a muffle furnace for 20 hours at 800°and 900°C and the produced materials were evaluated. The cubic structure of all $Cu_xCo_{1-x}Fe_2O_4$ ferrites was single-phase and closely matched the data from the standard JCPDS card no. 25-0283 and JCPDS card no. 17-

0464.[20,21].The lattice parameters for the samples $CoFe_2O_4$, a = 8.389 Å, $Cu_{0.4}Co_{0.6}Fe_2O_4$, a = 8.3744 Å and $CuFe_2O_4$, a = 8.2543 Å.

The schematic way of representation to find the magnetic properties using hysteresis loop is shown in Fig. 3. The hysteresis loop is drawn by plotting the magnetic field strength H against the magnetic induction B in the core material. If

3.2 Magnetic properties

a current is flowing through a coil, it will cause a magnetomotive force F. The magnetic properties of ferrites have be calculated using following equations:

$$F = \frac{magnetizationofnickelinemu}{verticaldisplacementonCROfornickelinmv} = \frac{102}{1010} = 0.10099\, emu/mv \cdots (1)$$

Then vertical displacement for each sample on CRO was noted to calculate the saturation magnetization by relations,

σ_s' = calibration factor X vertical displacement in mv = (f x v) emu ... (2)

$$\text{and } \sigma_s' = \frac{\sigma_s}{\boldsymbol{mass\ of\ sample}} emu/gm \cdots (3)$$

Similarly saturation magnetization in emu/cc was calculated using the relation

$$M_s = (1-p)\sigma_s' dx \cdots emu/cc \cdots (4)$$

Where p = porosity = $\frac{dx-da}{dx}$ dx = x - ray density, da = actual density

Lastly magnetic moment per molecular formula unit in Bohr magneton was calculated by the relation.

$$\mu_B = \frac{Molecularweight \times \sigma_s}{5585} \cdots Bohrmagneton \cdots (5)$$

$1\mu_B$= 5585 emu/mole

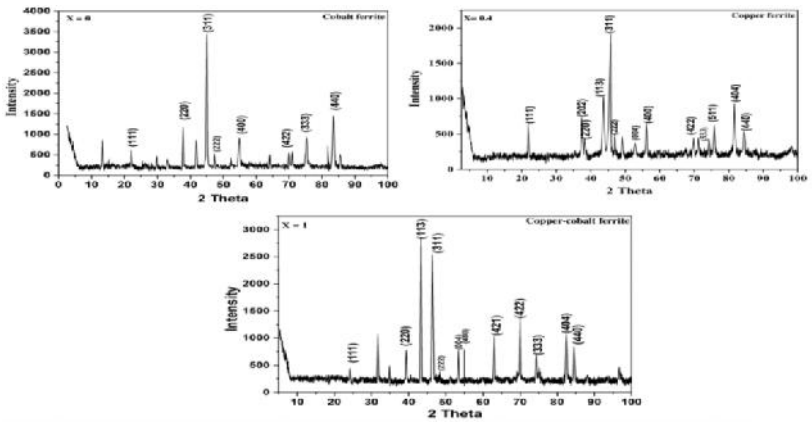

Figure 2 Refine Rietveld X-ray diffraction graphs for each sample

Figure 3 Schematic representation of magnetic

Table – 2: The data on composition, sintering conditions and CRO records

Composition X	Sample	Sintering temperature in c°	Sintering time in hours	CRO vertical record for hysteresis loop in mv	Porosity ° in %	Saturation magnetization M_s in emu/cc	Magnetic moment μ_B in Bohr magneton
0.0	$CoFe_2O_4$	800	20	850	32	308	3.714
		900		862	24	350	3.995
			30	905	20	386	4.041
0.4	$Cu_{0.4}Co_{0.6}Fe_2O_4$	800	20	136	30	111	1.306
		900		161	23	142	1.533
			30	170	15	158	1.482
1.0	$CuFe_2O_4$	800	20	270	34	48.9	0.7042
		900		326	31	60.0	0.9984
			30	341	29	65.0	0.8884

The calculated values of magnetization and magnetic moment are represented in Table 2. The sample fired at 900^{0}C for longer time show greater magnetization than others. This behaviour is attributed to redistribution of cations and microstructural changes brought in by firing conditions. At the same time the reduced porosity at higher sintering conditions has considerable effect in enhancing the magnetization of samples [22].

Prince et al [23] has reported inverse spinel structure in $CoFe_2O_4$ by neutron diffraction. In such a case the theoretical magnetic moment would be 3 Bohr magneton. As Zn^{2+} ions occupy tetrahedral sites, nickel (Ni^{2+}) ions occupy octahedral sites and manganite (Mn^{2+}) ions occupy tetrahedral sites. Cobalt (Co^{2+}) ions are reported to occupy A-sites up to a maximum of 10% in cobalt ferrite depending on the annealing temperature. From Mossbauer study of cobalt-zinc ferrite it has been observed that the amount of cobalt at A-site decreases from 10% with the increase of zinc content. However in the present examples it varies from 3.714 to 4.041 Bohr Magneton [Table-2].

This can be ascribed to the contribution of orbital and spin movement along with the degree of inversion. Sawatzky et al [24] have reported partial inverse spinel structure in Cobalt ferrite. Hence in the present case partial inverse spinel structure is assigned to Cobalt ferrite and accordingly cation distribution is given by From experimental values of μ_B for $CoFe_2O_4$, δ comes out to be 0.18, 0.24 and 0.26, depending on sintering conditions. Hence it can be concluded that normalcy varies from 15 to 30% depending on heat treatment.

$$\left(Fe^{3+}_{1-\delta}Co^{2+}_{\delta}\right)\left[Co^{2+}_{1-\delta}Fe^{3+}_{1+\delta}\right]O^{-2}_{4} \quad \ldots (6)$$

Where δ = coefficient of normalcy of cobalt ferrite <1.The resultant magnetic moment per formula is given by

$$\mu_B = 3 + 4\delta \quad \ldots (7)$$

The magnetic moment of $CuFe_2O_4$ ferrite is found to vary from 1.306 to 1.533 Bohr magneton [Table-2]. However theoretical value is only 1 Bohr magneton. The same behaviour was reported by earlier workers suggesting the partial inversion $CuFe_2O_4$ [25]. Hence in the present case, copper ferrite is supposed to have partial inversion spinel structure and accordingly the cation distribution is given by

$$\left(Fe^{3+}_{1-\delta}Cu^{2+}_{\delta}\right)\left[Cu^{2+}_{1-\delta}Fe^{3+}_{\delta}\right]O^{-2}_{4} \ldots (8)$$

Where, δ = coefficient of normally <1.The resultant magnetic moment of copper ferrite per formula unit is given by

$$\mu_b = 1 + 8\delta \quad \ldots (9)$$

From experimental values of μ_B for $CuFe_2O_4$ (Table-2), δ is found to vary from 0.0375 to 0.06662, leading to 93 to 97% of inversion, depending on sintering conditions which are supported by earlier results [26].The addition of copper to cobalt ferrite, makes the copper ions to occupy A sites, replacing Fe^{3+} ions, which in turn occupy B sites, as per site preference energies, vacating Co^{2+} ions. This results in the decrease of magnetization of A site, as copper is

diamagnetic in nature. Basically, as increase in Ms as x increases can be explained by the possible substitution of Co^{2+} by Cu^{2+} at the tetrahedral sites of the spinel ferrite lattice. These observed trends in the variation of Ms can be justified by Neel's two-sublattice magnetization model. According to Neel's two-sublattice magnetization model, magnetization (in μB) is given by M (μB) = $M_B - M_A$, where M_A and M_B are the net magnetic moments of A (tetrahedral) and B (octahedral) sites, respectively. The magnetic moment of Cu^{2+} (1μB) is less than that of Co^{2+} (3 μB) and due to the substitution of cobalt by copper at the tetrahedral sites, hence net magnetization increases. At higher levels of substitution (only cobalt ferrite) it is possible that part of cobalt is substituted at the octahedral sites so that the net magnetization decreases due to the decrease in the value of M_B[27,28].

The cation distribution at X=0.4 can be represented as

$$\left(Cu_{0.4}^{2+}Co_{0.4}^{2+}Fe_{\delta}^{3+}\right)\left[Co_{0.2}^{2+}Fe_{2-\delta}^{3+}\right]O_4^{-2} \quad \ldots\ldots(10)$$

From experimental results for Cu-Co ferrites, at X=0.4, the value of δ is estimated to be in between 0.97 and 0.998. Hence it can be concluded that A and B sites are almost equally occupied by Fe^{3+} ions and resultant magnetization is mainly due to ions at A sites which contribute small amount to magnetization. Hence observed magnetization is comparatively small. At higher sintering conditions, net area of grain boundary decreases due to densification and low porosity. As a result, the domain walls become more mobile to increase the magnetization. This implies that when crystallites become large with negligible porosity, crystalline anisotropy decreases and makes the magnetization easier one. Lower sintering temperature and time cause for many small grains whereas higher sintering conditions give rise to small number of large grains and consequently leads to low porosity. The domain structure is modified due to interaction between the neighbouring grains [29]. This leads to the linear relationship between permeability and grain diameter and causes for the increase in magnetization with increased grain diameter, whereas the decrease in magnetization at a low sintering temperature and time is attributed to the formation of closed pore chains which cause for diamagnetic field to decrease the magnetization [30-31].

Surface morphology

The maximal grain growth across in a sample sintered at 800^0 and 900^oC for 20 to 30 hours is shown from SEM micrographs (Figure-4). When closed pores become trapped inside the grains and become isolated from grain borders, they can no longer contract, which causes the excessive grain growth [22, 31-34]. According to SEM, there is agglomeration, and the crystals are spherical with irregular shapes and their size ranges from micro-meter size.It can be observed from the figures that theaverage grain size decreases with increasing copper concentration, which is because,the ionic radius of $Cu^{+2}$is smaller than that ofCo^{+2}. Therefore, the decrease in grain size may bedue to diffusion of copper during heat treatment [35]. Due of an uneven diffusion rate, the migration of vacancies from pore or grain borders results in the development of porosity at the base. Large grains could be a result of oxygen vacancies brought on by reduction during heat treatment. Large pores at grain boundaries are thought to be caused by metal ion vacancies brought on by oxidation or appropriate doping[36].Thus, it can be stated that the diameter of grains increases due to densification via decreasing porosity and increasing sintering temperature and duration.

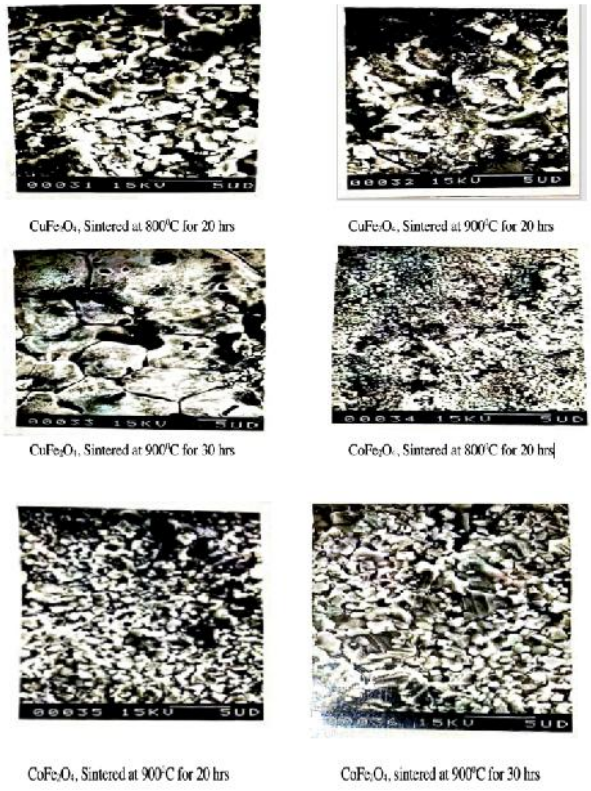

Figure 4 SEM images of the$Cu_xCo_{(1-x)}Fe_2O_4$ (x=0, 0.4 and 1) sintered at 800 and 900^0C

CONCLUSION

$Cu_xCo_{(1-x)}Fe_2O_4$(x=0,0.4, and 1.0) was synthesized using the traditional solid-state method and lattice constant lies in the range 8.2543 Å- 8.389 Å and confirms cubic structure. Morphological research reveals that the microstructure of the grains grows due to densification, lowering porosity and raising the temperature with sintering process. Higher sintering temperatures that result in a reduction in the grain boundary, which makes the domain walls more movable and increases magnetization. A lower sintering temperature results in a more significant number of tiny grains that form closed pore chains and provide a diamagnetic field that lowers the magnetization commonly used in high-density storage media, ferromagnetic fluids, catalysts, magnetic drug delivery systems.

REFERENCES

[1] Mahmoud,W.E., Al-Ghamdi, A.A., Bronstein L, M., 2020. Development of a new family of spinel nano-ceramic ferrites based on $Ni_{1-x}Ho_xFe_2O_4$ ($0 \le x \le 0.07$) via a 1,4-dithioerythritol assisted polyol technique, Mater Lett, 269, 127677,

[2] Hashim. Mohd .Alimuddin. Shalendra, Kumar.B H, Koo. Sagar E. Shirsath. Mohammed E, M., Jyoti Shah., Mar. 2012.Structural, electrical and magnetic properties of Co–Cu ferrite nanoparticles, J Alloys Compound, 518, 11–18.

[3] Sujatha, C. Venugopal Reddy,K. Sowri Babu K., Ramachandra Reddy A., Rao K, H., Apr. 2012. Structural and magnetic properties of Mg substituted NiCuZn Nano Ferrites, Physica B Condens Matter, 407(8) 1232–1237.

[4] Faraz A., Ahmad N, M., Feb. 2012. Electrical and magnetic properties of Zr^{4+} and Ni^{2+} ions substituted Mn-Cu spinel ferrites, J Supercond Nov Magn, 25(2) 169–174.

[5] Dietrich C., Hertel R., Huber M., Weiss D., Schäfer R., Zweck J., May 2008.Influence of perpendicular magnetic fields on the domain structure of permalloy microstructures grown on thin membranes, Phys Rev B Condens Matter Mater Phys, 77(17) 174427.

[6] Curély J., Barbara B., Jan. 2006.General theory of super-exchange in molecules, Struct Bond, 122, 207–250.

[7] Anderson,P.W,.1950.Antiferromagnetism. Theory of Super-exchange Interaction, Physical Review, 79(2) 350.

[8] Kolekar,R.Y,. Kapatkar.S,B., Mathad,S.N,. 2020. Nickel-Doped Cobalt Zinc Ferrites $Co_{0.8-x}Ni_xZn_{0.2}Fe_2O_4$ (x=0.0–0.56) by Solid-State Reaction: Synthesis and Characterization, International Journal of Self-Propagating High-Temperature, Synthesis, 29(4) 196–201.

[9] Bharamagoudar R.C., Patil,A.S., and Mathad,S.N.,2021.Structural, Dielectric, and Magnetic Properties of SCS-Produced Copper Zinc Nanoferrites, International Journal of Self-Propagating High-Temperature Synthesis, 30(4) *241–245.*

[10] Shirsath,S.E,. Wang, D., Jadhav, S.S., Mane,M.L.,S,Li. 2018. Ferrites Obtained by Sol–Gel Method. In: Klein, L., Aparicio, M., Jitianu, A*. (eds)* Handbook of Sol-Gel Science and Technology. Springer, Cham.

[11] Shashidharagowda,H., Mathad,S.N., Malladi,S., Gubbiveeranna, V.G., Patil,S.N,., Khan,A. Y.,Rub, M.A,., Asiri,A.M., Azum. 2021. Sol–Gel Co-Precipitation Synthesis, Anticoagulant and Anti-Platelet Activities of Copper-Doped Nickel Manganite Nanoparticles. Gels, 7(4*) 269.*

[12] Vishwaroop,R., Mathad,S.N. 2020 Synthesis, structural, W-H plot and size-strain analysis of nano cobalt doped $MgFe_2O_4$ ferrite, Sci. Sinter. 52, 1–10.

[13] Galagali,S.L.,Patil,R.A., Adaki,R.B., Hiremath,C.S., Mathad,S.N., Pujar,R.B. 2018. Influence of cadmium substitution in magnesium ferrites on structral and mechanical properties Sci. Sinter., 50, 217-223

[14] Singhal,S., Singh,J., Barthwal,S.K., 2005. Preparation and Charectrisation of Nanosize Nickel- Substituted Cobalt Ferrites $Co_{(1-x)}Ni_xFe_2O_4$, Solid State Chem., 178, 3183

[15] Rendale,M.K., Mathad,S.N., Puri,V. 2015. Thick films of magnesium zinc ferrite with lithium substitution: Structural characteristics, International Journal of

Self Propagating High Temperature Synthesis, 24, 78

[16] Patil, M.R., Rendale, M.K., Mathad,S.N., Pujar,R.B., 2015.Structural and IR study of $Ni_{0.5-x}Cd_xZn_{0.5}Fe_2O_4$,Int. J. Self-Propag. High Temp. Synth, *24, 24.*

[17] Molakeri,A., Kalyane,S., Kulkarni,A.B., Mathad,S.N. 2017. Elastic Properties of nickel ferrite synthesized by combustion and microwave method using FT-IR spectra, Int. J. Adv. Sci. Eng., 3, 422.

[18] Rakesh,M.S., Priyanka,P.K., Mahadev, R.S., Ashok, B.G., Pradip, D.K., Mathad, S.N., 2022. Synthesis and Characterization of Nd^{3+} Doped Mg-Cd Ferrite ($Mg_{0.5}Cd_{0.5}Nd_{0.01}Fe_{1.99}O_4$) Nanoparticles Prepared in the Form of a Thick Film for Gas Sensing Applications, Journal of Nano electronic Physics, 14(4) 04001.

[19] Kakati,S., Rendale,M.K., Mathad,S.N., 2021. Synthesis, Characterization, and Applications of $CoFe_2O_4$ and M-$CoFe_2O_4$ (M = Ni, Zn, Mg, Cd, Cu, RE) Ferrites: A Review, International Journal of Self-Propagating High-Temperature Synthesis, 30(4) 189–219

[20] Choudhari,N.J., Kakati,S.S., Hiremath,C.S., and Pujar,R.B., May 2016. Structure dependent electrical properties of Ni-Mg-Cu nano ferrites, AIP Conf Proc, vol. 1728,

[21] Kazi., Sadiya., Feeda,S., Kakati,S.S., Mathad,S.N., Jeergal,P.R.., Pujar,A.S., Hiremath,C.S., Galgali,S.L., Rendale,M.K., and Pujar,R.B., 2020. Sintering temperature dependent structural and mechanical studies of $Ba_xPb_{1-x}TiO_3$ferroelectrics, Journal of Nano- and Electronic Physics, 12, 04018

[22] Bharamagoudar, R.C., Patil, A.S., and Mathad,S.N., Structural, Dielectric, and Magnetic Properties of SCS-Produced Copper Zinc Nanoferrites, Oct. 2021.International Journal of Self-Propagating High-Temperature Synthesis, 30(4). 241–245.

[23] Prince,E., May 1956. Neutron Diffraction Observation of Heat Treatment in Cobalt Ferrite, Physical Review, 102(3) 674.

[24] Sawatzky,G.A.,Woude,F.V., Morrish, A.H., Nov. 2003. Cation Distributions in Octahedral and Tetrahedral Sites of the Ferrimagnetic Spinel $CoFe_2O_4$, J Appl Phys, 39(2) 1204.

[25] Zuo,X., Yang,A., Vittoria,C., and Harris,V.G., 2006. Computational study of copper ferrite ($CuFe_2O_4$), J Appl Phys, 99(8).

[26] Shashidharagowda, H., Mathad, S.N. ,Abbigeri, M.B., 2022. Structural, Vibrational and Magnetic Characterization of Copper doped $CoMn_2O_4$Nano-particles Synthesized by Chemical Route, Science of Sintering, 53(4)

[27] Kumar,A., Rao,P., Varma,M., Choudary,G., Rao,K., 2011. Cation Distribution in $Co_{0.7}Me_{0.3}Fe_2O_4$ (Me = Zn, Ni and Mn), Journal of Modern Physics, 2(9) 1083-1087.

[28] HypoliteM. K, Patrice K.T. ,RoussinL.F., Ekane P. E., Pattayil A. Joy, Arnaud D. John N.L., 2018. Structural characterization and magnetic properties of undoped and copper-doped cobalt ferrite nanoparticles prepared by the octanoate coprecipitation route at very low dopant concentrations, RSC Adv., 8, 38621-38630

[29] Bates,L.F., Clow,H., Craik,D.J., Griffiths,P.M., Aug. 1958 .Magnetization Processes in a Polycrystalline Manganese Zinc Ferrite, Proceedings of the Physical Society, 72(2) 224.

[30] Patil, M. R., Rendale, M. K. Mathad, S. N., Pujar, R. B., 2017. Electrical and magnetic properties of Cd^{+2} doped Ni-Zn ferrites, Inorganic and Nano-Metal Chemistry, 47:8, 1145-1149,

[31] Monika, 2020. Structural Electrical and Magnetic Properties of Lanthanum and Dysprosium Substituted Ferrite Based Nanomaterials Synthesized by Sol gel Technique, Shoolini University of Biotechnology and Management Sciences (Ph.D,Thesis).

[32] Singh,S., Goswami,N., Katyal,S.C., Jan. 2020. Magnetic and dielectric study of nanoparticles of Cu-ferrite prepared by explosion technique, Mater Today Proc, 28,294–297.

[33] Kalia,S., Kumar,A., Sharma,S., Prasad,N., 2022. Properties, applications, and synthesis of first transition series substituted cobalt ferrite: a mini review, J. Phys.: Conf. Ser. 2267 012133.

[34] Pujar,A.S., Kulkarni,A.B., Mathad,S.N., Hiremath,C.S., Rendale,M.K., Patil,M.R., Pujar,R.B. 2018., Structural, Electrical,

and IR Properties of $Cu_xCo_{1-x}Fe_2O_4$ (x = 0, 0.4, 1.0) Prepared by Solid-State Method, International Journal of Self-Propagating High-Temperature Synthesis, 27(3) 174–179.

[35] Zeeshan, T., Anjum,S., Iqbal,H., Zia,R., 2018. Substitutional effect of copper on the cation distribution in cobalt chromium ferrites and their structural and magnetic properties, Materials Science-Poland, 36(2) 255-263

[36] Chakradhary,V.K., Ansari,A., and Akhtar,M.J., 2016. Synthesis and characterization of nickel cobalt ferrite nanoparticles via heat treatment method, Advanced Materials Proceedings, 1(1). 76–80.